Nuclear Inst. and Methods in Physics Research, A 893 (2018) 1–9

Contents lists available at ScienceDirect

Nuclear Inst. and Methods in Physics Research, A

journal homepage: www.elsevier.com/locate/nima

Design of an ultrathin cold neutron detector

A. Osovizky [a,b,c], K. Pritchard [a], Y. Yehuda-Zada [d], J. Ziegler [a], E. Binkley [a], P. Tsai [a], A. Thompson [a], N. Hadad [a], M. Jackson [e], C. Hurlbut [e], G.M. Baltic [a], C.F. Majkrzak [a], N.C. Maliszewskyj [a,*]

[a] NIST Center for Neutron Research, Gaithersburg, MD, United States
[b] Rotem Industries Ltd, Rotem Industrial Park, Israel
[c] University of Maryland, College park, MD, United States
[d] Nuclear Research Center Negev, Beer-Sheva, Israel
[e] Eljen Technologies, Sweetwater, TX, United States

ARTICLE INFO

Keywords:
Scintillator
Neutron detector
LiF:ZnS(Ag)
Silicon photomultiplier
CANDOR

ABSTRACT

We describe the design and performance of an ultrathin (<2 mm) cold neutron detector consisting of ^{6}LiF:ZnS(Ag) scintillator in which wavelength shifting fibers have been embedded to conduct scintillation photons out of the medium to a silicon photomultiplier photosensor. The counter has a neutron sensitive volume of 12 mm wide × 30 mm high × 1.4 mm deep. Twenty-four 0.5 mm diameter wavelength shifting fibers conduct the scintillation light out of the plane of the detector and are concentrated onto a 3 mm × 3 mm silicon photomultiplier. The detector is demonstrated to possess a neutron detection efficiency of 93% for 3.27 meV neutrons with a gamma ray rejection ratio on the order of 10^{-7}.

1. Introduction

Neutron scattering is a well-established technique for exploring the structure and dynamics of condensed matter [1]. Traditional diffractometers and reflectometers at continuous sources use many means to select out and direct a monochromatic beam of neutrons onto a sample under study. Neutrons scattered from this sample are then detected by a neutron sensitive detector. Recently, neutron scattering instruments utilizing polychromatic beams at continuous sources have begun to be developed, e.g., the Chromatic Analysis Neutron Diffractometer or Reflectometer (CANDOR) spectrometer [2] at the NIST Center for Neutron Research (NCNR).

In such an instrument, a polychromatic ("white") incident beam of neutrons illuminates a sample and the resultant scattered neutrons pass through arrays of highly oriented pyrolytic graphic (HOPG) crystals set at different angles with respect to the centerline of the array. Neutrons of the appropriate energy are subsequently Bragg-diffracted by the crystals into an associated neutron detector. By collecting the scattered radiation in these discrete energy bins simultaneously, it will be possible to perform measurements much more efficiently than is currently possible on a traditional instrument of this type.

To achieve this enhanced rate of measurement (and to more efficiently use the neutrons produced by the source), it is essential to have as many of these energy-analyzing channels as possible packed into a tight angular range. If the neutron detector is exceedingly thin (~2 mm), the spectrometer can accommodate numerous analyzing channels.

The ^{3}He gas filled proportional counter has been a mainstay technology for neutron detection for decades. It exhibits excellent gamma rejection and its neutron sensitivity can be tuned by adjusting the pressure of the counting gas mixture. Unfortunately, it is exceedingly difficult to design a pressure vessel of the appropriate dimensions to support so thin a counter with the desired sensitivity (>85% for 5 Å neutrons). This fact, coupled with the worldwide shortage of this strategic material prompted us to investigate alternative technologies for the neutron sensor.

Several groups have developed neutron detectors using ^{6}LiF:ZnS(Ag) scintillator read out with wavelength shifting fibers. Several groups have manufactured position sensitive detectors using arrangements of wavelength shifting fibers running along the surface of a scintillator sheet [3–6]. Others have looked to this technology to create a substitute for ^{3}He gas filled tubes for neutron diffraction and spectroscopy [7,8]. As mentioned above, a leading requirement in the CANDOR application is the minimization of the detector thickness to increase the number of energy analyzing arrays in the analyzer package.

* Corresponding author.
E-mail address: nicholas.maliszewskyj@nist.gov (N.C. Maliszewskyj).

https://doi.org/10.1016/j.nima.2018.02.073
Received 19 September 2017; Received in revised form 14 February 2018; Accepted 15 February 2018
Available online 2 March 2018
0168-9002/Published by Elsevier B.V.

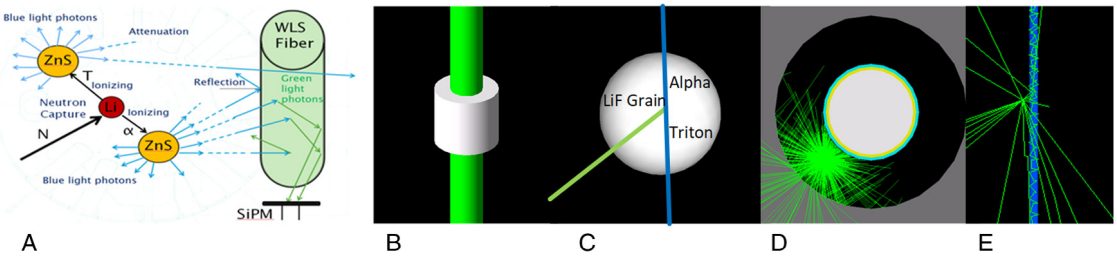

Fig. 1. A—Schematic illustration of the detection process starting with the neutron capture, ionization and light transport. B—Geometrical simulation of the fiber and scintillation mixture. C—Interaction between neutron and LiF grain. D—Blue light photons transported from a neutron capture occurring 0.35 mm from the center of the fiber (only 7.6% of the light reaches the fiber compared to 15.8% when the neutron capture occurs 0.3 mm from the center of the fiber. E—Light transport in the WLS fiber – only 5% of the green light created in the WLS fibers reaches the SiPM light sensor.

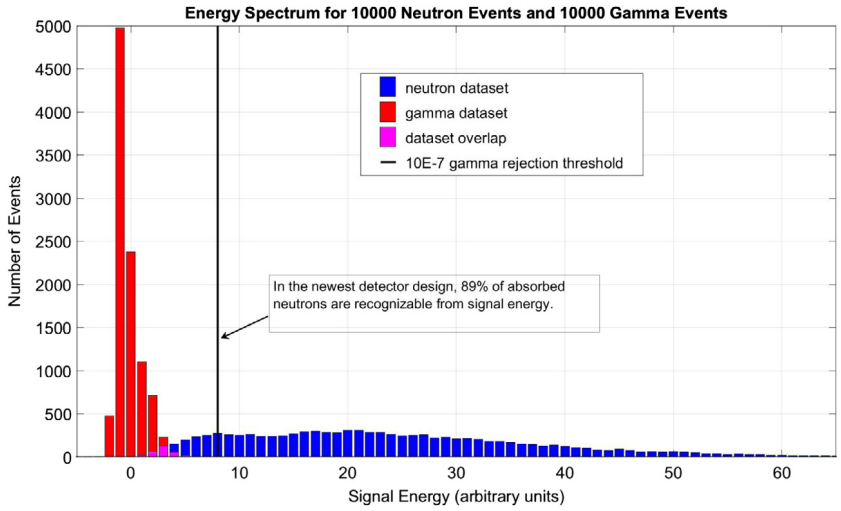

Fig. 2. Distributions of gamma and neutron events. Notice the large number of neutron events that are below the PHD threshold. Pure gamma datasets were acquired using isotopic ^{137}Cs.

2. ^{6}LiF:ZnS(Ag) detector design

Our concept for an ultrathin neutron detector consists of slabs of ^{6}LiF:ZnS(Ag) scintillator which have been formed around an array of wavelength shifting (WLS) fibers. The fibers are bundled together and run to a silicon photomultiplier (SiPM) to detect the scintillation light. The raw signal from the SiPM is amplified and digitized by fast ADCs. The resulting waveform is then processed by a field programmable gate array to discriminate neutron capture events from other signal sources.

Within the ^{6}LiF:ZnS(Ag), a neutron captured by a ^{6}Li produces an alpha particle and triton with a kinetic energy of 4.7 MeV [9–11]. The alpha particles and tritons travel for a few microns ($\alpha \sim 0.007$ mm, $T \sim 0.04$ mm) [12,13], losing energy and ionizing the ZnS(Ag) phosphor. This ionization produces up to 170,000 photons per neutron capture with a luminescence wavelength of 450 nm. The ZnS(Ag) phosphor can also be ionized by gamma rays (75,000 photons/MeV). The distinction between the two is that a gamma capture event is short lived (<200 ns) and a neutron capture event can be quite long lived (between hundreds of ns and ten μs). In addition, the scintillator itself exhibits an afterglow which can last for more than 100 μs. Thermal noise events in the photosensor are very short lived (<20 ns).

An array of 0.5 mm wavelength shifting (WLS) fibers [14] have been embedded in the scintillator to collect the scintillation light and conduct it to a photosensor out of the plane of neutron capture. The dye in the WLS fibers (650 ppm) absorbs the blue light photons and emits green light photons which travel down the fiber to a miniature solid state photosensor (SiPM) [15]. This arrangement offers the thinnest possible detector configuration and allows the detector thickness in the design requirement to be realized.

Although the raw number of photons emitted per neutron capture can be very large, the measurable amplitude of the light signal from this event can be quite low for several reasons. Only a small fraction of the photons is emitted in the direction of the WLS fiber. The efficiency of the fiber for capturing, converting, and guiding photons via the fiber is only about 5% for fibers with multiple cladding. Furthermore, the well-known opacity of ZnS(Ag) to its own scintillation light further reduces the number of photons which can even reach the WLS fibers depending on the location of the capture event within the scintillator, see Fig. 1. This can result in a distribution of the signal strength varying by as much as two orders of magnitude.

3. Signal processing

Because the intensity of the signal for gamma and neutron events can be similar, pulse height discrimination techniques are insufficient to discriminate neutron events from other signal types (Fig. 2). Pulse shape discrimination is much more sensitive as it can better differentiate the signal types based on the decay of the waveform [16,17]. Fig. 3 demonstrates that for two different waveforms varying markedly in their amplitude it is still possible to correctly identify a neutron. In our studies, we used a pulse shape discrimination technique using two integration windows defined relative to the rising edge of the waveform ($t = 0$ ns): a prompt integration window (0–200 ns) and a delayed (or tail) integration window (200–2000 ns).

In order to serve as a practical alternative to ^{3}He gas filled detectors, each scintillator detector must be able to discriminate neutron capture events at rates exceeding 10 kHz. Event pileup is a real barrier to the ability to count at even these rates. The tail of a particularly strong

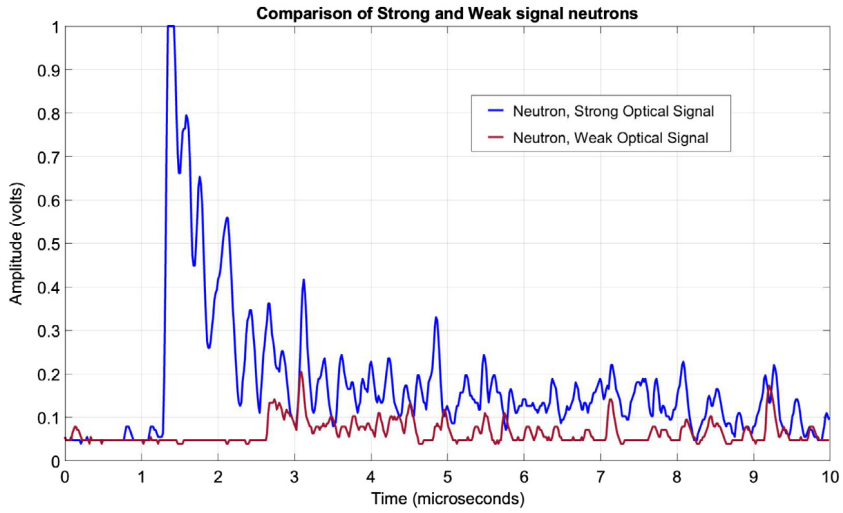

Fig. 3. Typical waveforms for strong (blue) and weak (red) neutron capture candidate events. (For interpretation of the references to color in this figure legend, the reader is referred to the web version of this article.)

neutron capture signal can maintain considerable intensity for durations exceeding 20 μs. During this interval, it is possible that gamma capture or thermal events (or even the stochastic burst of photons from the same neutron capture event) could be incorrectly interpreted as a neutron as they are superimposed on this long tail. Fig. 4 illustrates this possibility. The net result is that neutron capture events will be counted more than once.

One strategy to cope with the phenomenon of multiple counting is to add an inhibit time of several microseconds after the successful processing of a neutron event, but this will necessarily limit the event processing rate of the system. To enable the ability to process high neutron fluxes, the integration time of an event should be short relative to the desired count rate. Based on Eq. (1) the true neutron rate N_t is 10% higher than the measured neutron rate N_m for a neutron flux of 10,000 neutrons per second and a dead time τ of 10 μS. The sensitivity reductions for preset dead time and neutron flux can be evaluated based on the following equation [18].

$$N_t \cong N_m / \left(1 - N_m * \tau / T\right) \quad (1)$$

where:

N_t—true neutron rate
N_m—measured neutron rate
t—dead time
T – measurement interval

When using the equation with a dead time of 10 μs and a flux of 10,000 neutrons per second, about 10% of the events are statistically lost. This problem can be addressed by employing a detection algorithm with an adaptive inhibit time and trigger threshold level, to be described in a forthcoming manuscript [19].

Using a benchmark setup of SiPM, preamplifier, shaping amplifier, and multichannel analyzer, we determined that the area under the curve for a single pixel discharge of the SiPM was approximately 0.005 V μs. Typical photopeaks associated with neutron capture fell around 0.609 V μs while minimally detectable neutron captures fell lower, at about 0.191 V μs, or 40 photons.

4. Methods

Preliminary measurements with the prototype detector indicated that the scintillator absorbed about 90% of the incident flux (3.27 meV neutrons at our test station), but that the light output was low so the net sensitivity was only about 45%. Improvements in performance would require optimizations of the scintillator, the geometry of the WLS fibers,

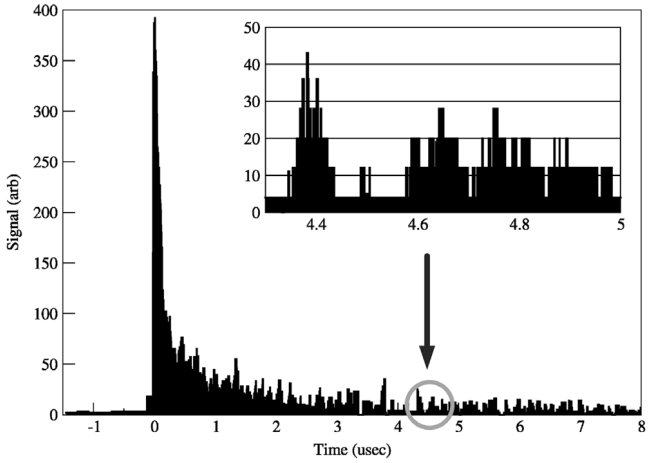

Fig. 4. The long tail of an event with a large amplitude could be interpreted as the signature of another, weaker neutron capture event.

the application of optical reflectors, and selection of the appropriate photosensor.

The overall neutron detection sensitivity is driven by neutron absorption in the scintillator, the transport of the scintillation photons to a photosensor, and the photodetection efficiency of the photosensor. The sensitivity was determined by comparing the output of the signal processing chain for the scintillator detector with a 1 inch (2.54 cm) diameter ^{3}He gas filled proportional counter used as a reference. The sensitivity of the ^{3}He tube was determined through gold foil irradiations to be about 94% for 3.27 meV cold neutrons.

Fig. 5 shows the measuring apparatus at the NG1 detector test station at the Center for Neutron Research. The reference detector was used to measure the neutron absorption of the scintillator detector under test.

An additional diagnostic measurement is the accumulation of a pulse height spectrum for the SiPM signal. While the pulse height is of limited utility in discrimination of neutron events from gamma or thermal events, it can be used as a measure of the light output of the scintillator.

For gamma rejection measurements, we used isotopic ^{137}Cs and ^{60}Co sources of known activity placed directly on the scintillator in the absence of neutrons (reactor off). We counted the number of candidate neutron events passed through by the pulse shape discriminator per hour and divided by half the source activity over the same period.

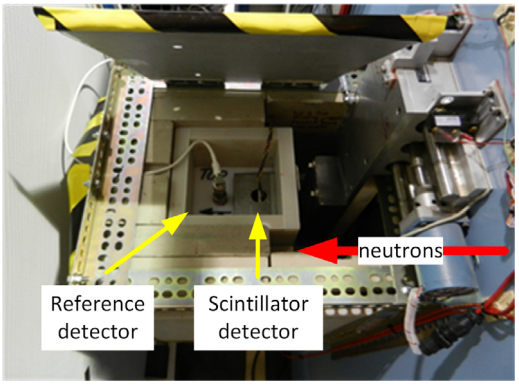

Fig. 5. Top down view of detector test box on the NG1 beam line at the NIST Center for Neutron Research.

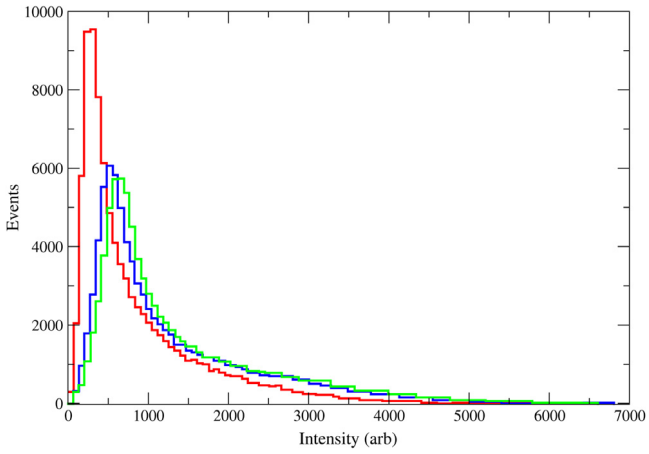

Fig. 6. Simulation of the light spectra for detector configurations of 12 fibers (red), 20 fibers (blue), and 20 fibers with a reflector (green). (For interpretation of the references to color in this figure legend, the reader is referred to the web version of this article.)

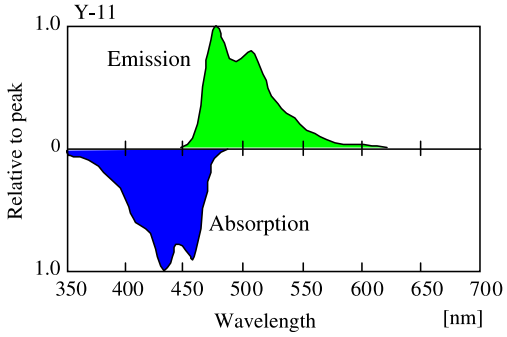

Fig. 7. Absorption and emission curves for Kuraray Y11 WLS fiber. (For interpretation of the references to color in this figure legend, the reader is referred to the web version of this article.)

5. Design studies

While initial efforts to select the appropriate scintillator stoichiometry focused on larger proportions of ^{6}Li, such prototypes displayed low sensitivity (~30%) despite having large neutron absorption (~97% at 3.27 meV). These results pointed us in the direction of improving light production and transport. We found that increasing the weight proportion of the putatively inert binder improved the light transmission for all wavelengths of visible light. We increased the binder fraction to 0.6, but found that further increases in the binder fraction (to 0.75) did not result in a commensurate increase in light transmission. Clearly other strategies (e.g., changing the geometry and number of WLS fibers) would have to be pursued to obtain additional gains.

The detector sensitivity is determined by the probability for neutron capture (Li concentration), the amount and temporal distribution of the light produced by ZnS(Ag) [20–22], the light transport properties of the scintillator (including binder concentration), the light collection properties of the WLS fibers, the ability of the WLS fibers to transport the light to the photosensor, and the ability of the photosensor to detect the light.

Using observations from these initial prototypes, we performed GEANT4 simulations [23] to explore many new detector configurations. Fig. 6 presents a simulation of the light spectra for 1 mm thick detector configurations with 12 fibers, 20 fibers, and 20 fibers with a Vikuiti reflector. The goal of these simulations was to find configurations that would permit us to detect the largest possible fraction of neutrons which were captured in the scintillator. We determined that increasing the number of WLS fibers in the detector improved the sensitivity at the cost of reducing the absorption of incident neutrons in the medium. We then explored tuning the thickness of the detector to increase the neutron absorption.

The results of simulations are summarized in Table 1. The overall neutron detection sensitivity is optimized for stoichiometries based on a 1:2 ^{6}LiF:ZnS(Ag) weight ratio. The simulation indicates that by increasing the number of fibers we can achieve the goal of high neutron absorption and very high (~97%) light collection efficiency such that every neutron captured in the scintillator may be detected. For a neutron to be considered detected our simulations used a threshold of 2300 photons.

The main purpose of the WLS fiber is to collect light from a thin tile-shaped scintillator by trapping the light and re-emitting the light in the fiber for transport. The wavelength shifting capture efficiency can be calculated per Eq. (2) [24] where C is the dye concentration; Kp is a constant set for each wavelength, and d is the fiber diameter.

$$I(\lambda) = I_0(\lambda) \times 1\text{–}10^{-(Kp*c*d)} \quad (2)$$

The challenge of building an ultrathin scintillation detector using such an opaque medium requires the optimization of the number and placement of the WLS fibers. We have investigated minimizing fiber diameter and increasing the concentration of the dye in the fiber. While higher dye concentrations in the fiber increase its efficiency for capturing the blue scintillation photon, they increase the likelihood of attenuating the transported signal (Fig. 7).

We selected Kuraray's Y11 WLS fiber for our neutron detector. We used a double clad version of the fiber to minimize attenuation losses in the fiber itself and selected an overall fiber thickness of 0.5 mm to maintain a thin detector. This small diameter fiber has poor capture efficiency (72.5%) when the standard 200 ppm dye concentration is used. By increasing the concentration of the dye to 650 ppm, the capture efficiency increases to 98.5%. We measured the transmission of light over 50 cm fiber lengths and found that the attenuation in the 650 ppm fiber was ~10% greater than for the 200 ppm fiber. (See Table 2.)

Through our study it became apparent that in using the ^{6}LiF:ZnS(Ag): binder as the scintillator in an ultrathin neutron detector, the most important optimization is the balance between the neutron capture probability and scintillation light transport. The greatest enhancement to light collection is achieved through proper arrangement of the WLS fibers in the medium. Fig. 8 presents the results of a GEANT4 simulation of light collection in our detector. Each dot represents a neutron capture event for which the number of scintillation photons exceeding a threshold are successfully captured in the WLS fiber. It is clear in both diagrams that most events producing detectable light are concentrated on the leading edge of the scintillator slab. The figure shows that if the photon detection threshold is increased from 200 to 2000 photons

Table 1
Simulation results aimed to determine an optimal detector configuration.

Detector configuration	Weight ratio (LiF:ZnS:binder)	No. of WLS Fibers	Reflector	Total sensitivity	Neutron capture probability	Light collection efficiency
1 mm thickness	1:2:0.3	12	Air	60.9	94.3	64.6
1 mm thickness	1:2:0.45	12	Air	69.4	93.3	74.4
1 mm thickness	1:2:0.6	12	Air	80.9	91.6	88.3
1 mm thickness	1:2:0.6	16	Air	85.8	89.9	95.4
1 mm thickness	1:2:0.6	20	Air	86.1	87.9	98.0
1 mm thickness	1:2:0.6	20	Vikuiti	87.0	87.9	99.0
1.1 mm thickness	1:2:0.6	20	Air	85.3	91.4	93.3
1.05 mm thickness	1:2:0.6	20	Air	86.5	89.8	96.3
1.1 mm thickness	1:2:0.6	20	Vikuiti	88.5	91.3	96.9
1.1 mm thickness	1:2:0.6	16	Vikuiti	85.2	92.8	91.8
1.1 mm thickness and 8 μm ZnS(Ag) layer on the front side	1:2:0.6	20	Vikuiti	89.7	91.4	98.1
1.1 mm thickness and 8 μm ZnS(Ag) layer on the front side	1:2:0.6	20	Alanod	89.2	91.4	97.6
1.1 mm thickness and 8 μm ZnS(Ag) layer, fibers are shifted 100 μm to the front side	1:2:0.6	20	Alanod	89.7	91.4	98.1

Table 2
Blue light (430 nm) capture efficiency.

Kp	**0.00638**	0.00638	0.00638	0.00638	450 nm
C	**650**	200	500	850	Dye concentration
d	**0.44**	0.44	0.44	0.23	Net diameter without the cladding
Trapping efficiency Eq. (2)	98.5	72.5	96.1	94.3	

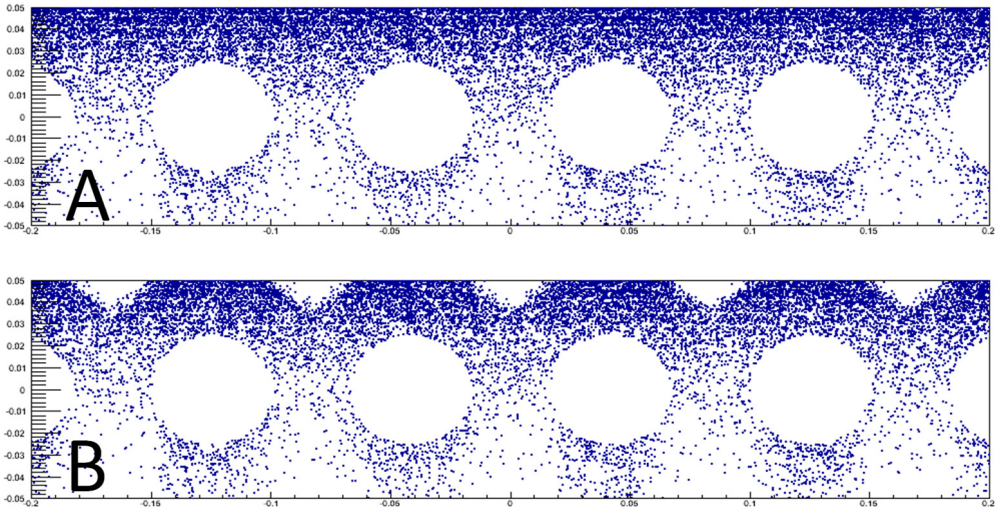

Fig. 8. Simulation made with GEANT4. A—The interaction location of events that produce light signature above a threshold level of 200 photons. B—The interaction location of events that produce light signature above a threshold level of 2000 photons.

entering the fiber there are pockets in that leading edge which do not contribute to the overall neutron count. Thus, our optimized (and more easily manufactured) configuration places the WLS fibers side by side so that they touch.

6. Reflector

Significant gains in performance can be realized by incorporating reflectors into the detector geometry. Neutron capture events occurring at the very edge of the scintillator are the most difficult to sense as fully half the photons produced are emitted in a direction away from the light collecting fibers and those emitted in the direction of the fibers must travel through more of the largely opaque scintillator. Reflectors at the leading and trailing faces of the scintillator will redirect photons back to the WLS fibers. In the GEANT4 simulation we found that the addition of reflectors increased the sensitivity from 85% to 88%.

Dramatic changes can be seen when a Vikuiti reflector is added to the outside faces of the scintillator slab (Fig. 9). While the total number of events for each curve is similar, the addition of the reflector shifts the distribution of photons to higher energies. A reflector on the front face (red curve) has the greatest effect. Adding a second reflector to the rear face provides a small enhancement.

We evaluated both Vikuiti ESR film [25] and Alanod Miro [26] backing as reflectors. The Vikuiti film has excellent specular reflectivity, but because it is a polymer product it contains a large proportion of hydrogen which can scatter neutrons before they are absorbed in the scintillator. The Alanod Miro-Silver film also has excellent reflectivity, but is based on an anodized aluminum and therefore is less likely to scatter neutrons. Our tests demonstrated that a Vikuiti film on the leading face of the detector scattered fully 2% of the incident neutrons, leading to a misleadingly low net sensitivity. Placing the Alanod film on the leading face did not result in such losses. The current configuration of the detector places Alanod on the leading face of the detector and Vikuiti on the trailing face.

Another type of reflector that bears mentioning is a reflector for the light transported via the WLS fiber. As a single photosensor is used to read out the scintillation light, that sensor is located out of the plane of the scintillator at a point where the WLS fibers may be concentrated.

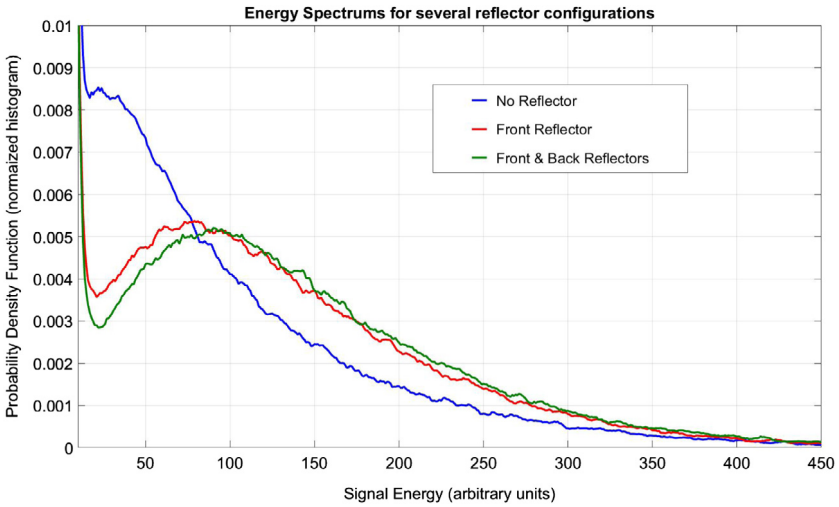

Fig. 9. Light spectra measured with and without Vikuiti reflector. The huge enhancement of the light signature improves neutron detection; however, the Vikuiti contains a high hydrogen concentration that scatters about 2.5% of the cold neutrons. (For interpretation of the references to color in this figure legend, the reader is referred to the web version of this article.)

The other end of the fiber can be terminated with or without a reflector. A configuration that we have used is a simple loop in the fiber which acts as a perfect reflector. We have found that this configuration leads to better light transport even though it uses more than twice the amount of WLS fiber. Performance tests indicate that the configuration with the loop provides a 3% net gain in neutron detection sensitivity over configurations in which the loop has been cut.

7. Detector block design

We elected to take a layered approach to building up the detector. A row of WLS fibers packed side by side is placed just slightly towards the front of the sensor to take advantage of the greater proportion of neutron capture events taking place there. The fibers are then coated with a thin "primer" layer of scintillator with a higher proportion of ^{6}LiF (1:2:0.6 ^{6}LiF:ZnS(Ag):binder) to increase the probability of neutron capture while reducing the amount of light produced per event. Thicker slabs of bulk scintillator backed on a reflector are then pressed into that primer layer, which also serves the purpose of adhering these layers of scintillator together.

The primer layer of scintillator is doped with nickel to shorten the decay time of light produced in a neutron capture event [27,28]. Capture events near the WLS fibers will produce a great deal of light which could potentially be counted as more than a single neutron. The primer layer is thin (~50 μm on each side of the fibers). The weight ratio for this layer was selected as 1:2:0.6 to increase the probability for neutron capture while the amount of light produced in each interaction is less important because of the geometrical proximity of the event and the WLS fibers.

The second layer is the detector main bulk layer. The detector sensitivity is strongly affected by a tradeoff between neutron capture probability and light transport; hence the mixture weight ratio for this layer was considered. Simulations of the scintillator detector indicated that if the thickness of the sensor is increased slightly and the density of ^{6}LiF absorbers is decreased, we would experience gains in light generation and collection. Fig. 10 shows pulse height distributions for two samples (1.1 mm thick 1:2:0.6 and 1.35 mm thick 1:3:0.6) with the same neutron absorption. The amount of light detected in the thicker sample was greater, leading to a greater likelihood that a captured neutron will be detected.

An enhancement we considered was the addition of a thin layer (~8 μm) of ZnS(Ag) phosphor to increase the light yield from neutron capture events occurring on the outside edges of the bulk scintillator slabs. While our early testing of this feature was promising, offering a net gain of 3% overall neutron sensitivity, the technical challenges associated with manufacturing working sensors with this thin layer were significant. The final versions of our sensors do not include this feature.

In the CANDOR detector bank the width of the beam down the array is 10 mm. Projecting the takeoff angle due to Bragg diffraction from each analyzer crystal on to the sides of the array we arrived at a maximal width for each sensor of 12 mm. For the sake of modularity, we packaged three sensors side by side in a triple frame in an overall width of 5 cm. For the sake of manufacturability, those three sensors are formed in a single large window. Crosstalk between sensors is prevented by ensuring that WLS fibers from adjacent detectors are no closer than 1.7 mm, longer than the maximal free path light in the scintillator.

The coupling between the WLS fibers and the SiPM [29] is achieved using a machined "fiber block". The WLS fibers are bundled into an area smaller than the active area of the SiPM and epoxied in place. The fibers are first cut with a hot knife just above the plane of the block and are then polished using successively finer grits of sandpaper until they are flush with the metal. The SiPMs are located on a printed circuit board which registers them with respect to the placement of the fiber bundles. A thin layer of optical grease is applied between the SiPM and fibers to make the optical connection between them. A schematic of this design both with and without the "perfect reflector" fiber loop is shown in Fig. 11.

8. Comparing detector performance

An optical Figure of Merit (FOM) was used to gauge the optical yield from a detector. We have tested several equations for the FOM (a unitless shape score) that scales with the light output of a scintillator, but also remains constant as a function of electrical gain of the preamplifiers, SiPM voltage, and shaping amplifier gain. The FOM determined in Eq. (3) represents a constant value with only ±5% change over a range of gain alteration up 300%.

By dividing the counts of different regions of the spectrum the equation is also normalized to the total number of counts.

$$\mathrm{FOM} = \left(\frac{Photopeak\ Channel}{Valley\ Channel}\right) \times \left(\frac{Photopeak\ Intensity}{Valley\ Intensity}\right) \tag{3}$$

We base our comparison of detector configurations on the principle that a higher optical FOM corresponds to a higher average photon yield. We found that detectors with an optical FOM of 10 or greater reliably have better identification of absorbed neutrons using a digital pulse shape discriminator with a gamma rejection ratio on the order of 10^{7}

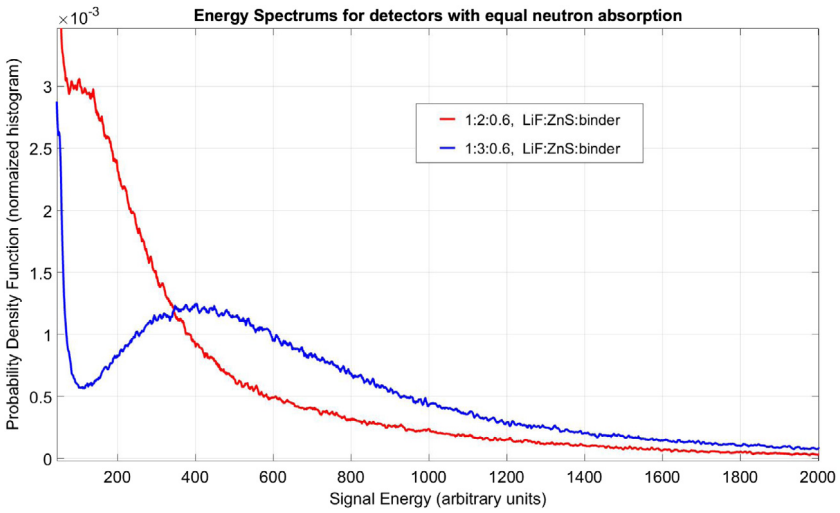

Fig. 10. Pulse height distributions measured for scintillators with ratios of 1:3:0.6 (blue) and 1:2:0.6 (red). Both samples have thicknesses tuned such that the neutron capture probability is 90% for 3.27 meV neutrons. (For interpretation of the references to color in this figure legend, the reader is referred to the web version of this article.)

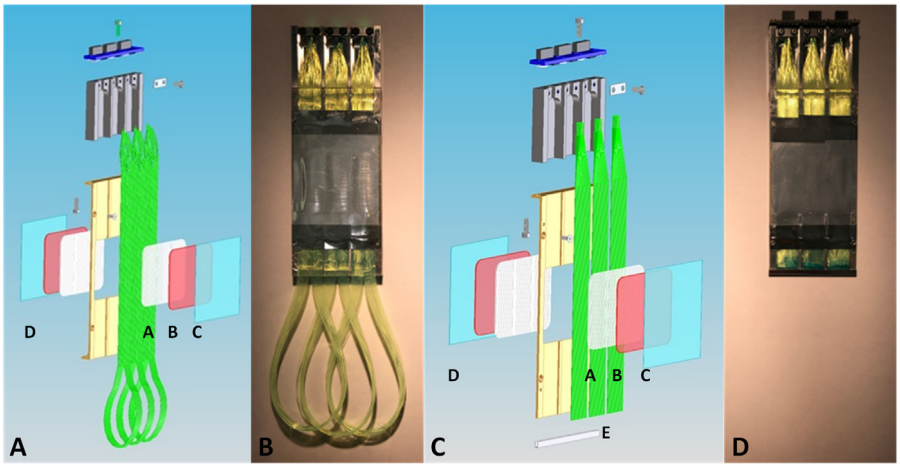

Fig. 11. Exploded assembly diagrams and photographs of the triple frame neutron detector in two different configurations. A: Exploded assembly of triple frame with a loop. Layer "a" consists of a 1:2:0.6 Ni-doped scintillator "primer". Layer "b" is a slab of 1:2:0.14 scintillator. Layer "c" is the Alanod reflector on the leading face. Layer "d" is the Vikuiti reflector on the trailing face. The SiPMs are mounted on a carrier board mating to the WLS fibers (e). B: Photograph of triple frame with the fiber loop. C: Exploded view of the triple frame with a terminal reflector (f) on the frame end. D: Photograph of triple frame with terminal reflector.

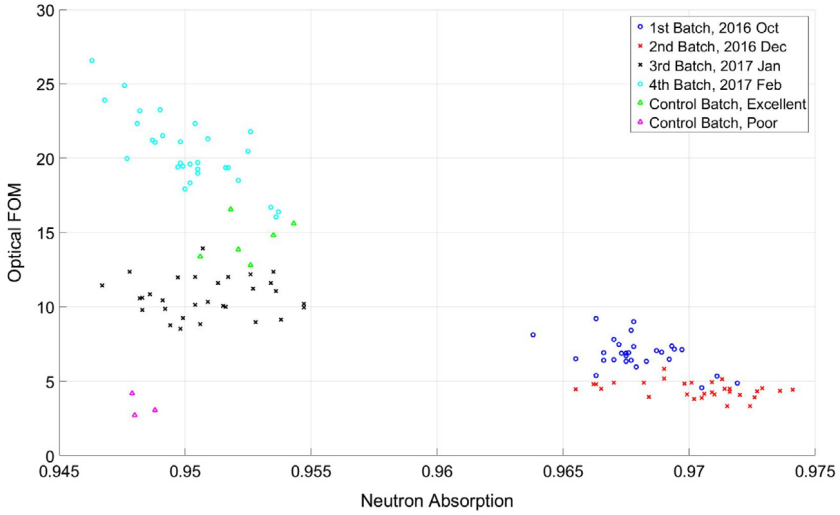

Fig. 12. Neutron absorption versus optical FOM for four different batches of sensors.

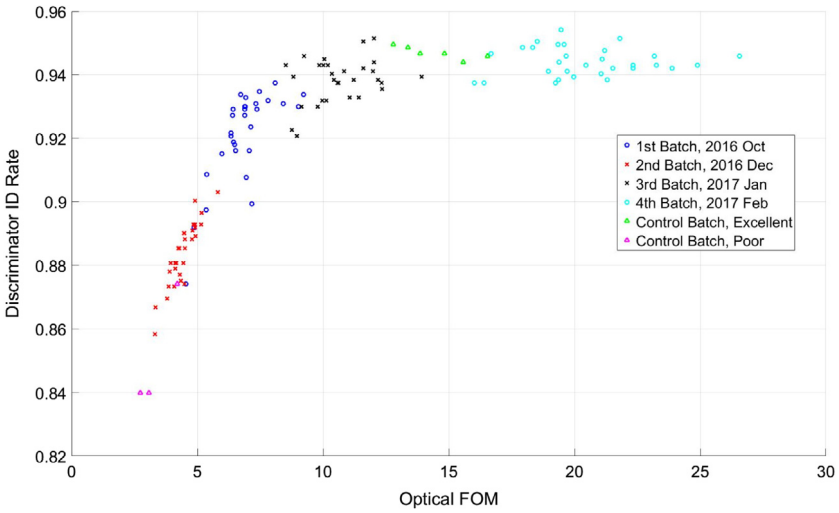

Fig. 13. Neutron identification rate (neutron events discriminated/neutrons removed from beam flux by scintillator detector) as a function of optical FOM for four different batches of sensors.

and very high probability of producing a distinguishable signal for every captured neutron.

Fig. 12 plots the neutron capture probability versus the optical FOM for four production batches, each of which consists of more than 25 detectors. The goal of an optical FOM above 10 was achieved on the third batch (black dots) by optimizing the mixture and slightly reducing the probability for neutron absorption (~2%) to a range of 85% and improving the light transport to the desired FOM. The absolute neutron capture probability was estimated based on our testing box described in Fig. 6 and a gold foil activation measurement. The figure also shows that the procedures set for the production process resulted in a quantity of scintillators with relatively uniform performance (neutron absorption and FOM).

Fig. 13 shows the probability for detecting a neutron which has been captured by the sensor. Not all the neutrons absorbed by the detector are detected.

We compared the number of events counted by our pulse shape discriminator with the number of neutrons that we believe were absorbed by the detector. This ratio is the Discriminator Conversion Efficiency. The Discriminator Conversion Efficiency increased, until the optical FOM reached a value of 10. Above 10, the discriminator conversion efficiency plateaus indicating that nearly all absorbed neutrons were counted.

Summary

We present the design and performance of an ultrathin (~1.5 mm) neutron sensitive detector using ^{6}LiF:ZnS(Ag) scintillator with a wavelength shifting fiber readout. The scintillation light is read out using silicon photomultipliers as the photosensors and the resulting signal processed using pulse shape discrimination techniques. Prototypes we have tested thus far exhibit 94% neutron absorption and greater than 93% neutron sensitivity for 3.27 meV neutrons. Simulations indicate that by stacking layers of our detector we could obtain sensitivities exceeding 90% for thermal neutrons as well. Pulse shape discrimination has resulted in excellent gamma rejection (2×10^{-7}) measured using isotopic gamma sources.

The structure of the scintillator proper is driven by the competition between neutron absorption and scintillation light transport and collection. Layers of scintillator material have been crafted to maximize the likelihood that scintillation photons from neutron capture events occurring far from the WLS fibers will travel through the medium to the WLS fibers where they will be collected. Reflectors added to the leading and trailing faces of the scintillator slabs enhance the probability that photons produced in neutron capture at the boundary of the scintillator are reflected towards the WLS fibers where they can be collected. WLS fibers are spaced close together to eliminate "dead" spaces in the scintillator.

When the neutron detectors are both exceedingly thin (~1–2 mm) and highly efficient (93% for 3.27 meV neutrons), it is possible to position many of energy-analyzing channels of the CANDOR spectrometer side by side. With a large bank of energy analyzing channels it will be possible to collect entire reflectivity curves in just a few settings of the spectrometer, allowing not only greater throughput for standard structural measurements but also possibly enabling classes of time resolved measurements which have heretofore not been practical. Furthermore, we estimate that this detector design has the potential to become a building block for other neutron detection applications by providing high performance and an affordable alternative to the ^{3}He gas-filled proportional counter.

Disclaimer

Certain trade names and company products are identified to adequately specify the experimental procedure. In no case does such identification imply recommendation or endorsement by the National Institute of Standards and Technology, nor does it imply that the products are necessarily the best for the purpose.

This work benefitted from the Center for Neutron Research at the National Institute of Standards and Technology; this facility is funded by the U.S. Department of Commerce.

References

[1] N.J. Rhodes, Scintillation detectors, Neutron News 23 (2012) 26–30.
[2] http://www.ncnr.nist.gov/instruments/CANDOR, [Online].
[3] D.P. Hutchinson, R.K. Richards, D.E. Holcomb, Position sensitive neutron detectors using a crossed fiber readout array, Proc. SPIE 3769 (1999).
[4] A. Stoykov, J.-B. Mosset, U. Greuter, M. Hildebrandt, A SiPM-based 6LiF:ZnS scintillation neutron detector, Nuclear Instrum. Methods Phys. Res. A 787 (2015) 361–366.
[5] A. Gorin, K. Kuroda, I. Manuilov, Development of a scintillation imaging device for cold neutrons, Nuclear Instrum. Methods Phys. Res. A 479 (2002) 456–460.
[6] C.L. Melcher, Perspectives on the future development of new scintillators, Nuclear Instrum. Methods Phys. Res. A 537 (2005) 6–14.
[7] B. Tang, Z. Sun, Q. Zhang, Study of a position sensitive scintillation neutron detector, Chinese J. Phys. 36 (11) (2013) 1089–1094.
[8] A. Stoykov, J. Instrum. 9 (2014) 6015.
[9] C.W.E. Van Eijk, Neutron psds for the next generation of spallation neutron sources, Nuclear Instrum. Methods Phys. Res. A 477 (2002) 383–390.

[10] C.W.E. Van Eijk, Inorganic scintillator development, Nuclear Instrum. Methods Phys. Res. A 460 (2001) 1–14.
[11] V.S. Litvin, A.D. Beyaev, S.M. Ignatov, ZnS(Ag)/6LiF and LiI(Eu) scintillaotrs and silicon photomultipliers for thermal neutron dete3ctors with high space and time resolution, Bull. Russ. Acad. Sci. Phys. 73 (2009) 219–221.
[12] W. Chong, B. Tang, Z. Sun, Q. Zhang, W. Luo, T. Wang, The Monte Carlo simulation on a scintillator neutron detector, Sci. China Phys. 56 (10) (2013) 1892–1896.
[13] D.S. McGregor, M.D. Hammin, Y.H. Yang, Design considerations for thin film coated semiconductor thermal neutron detectors, Nuclear Instrum. Methods Phys. Res. A 500 (2003) 272–308.
[14] http://kuraraypsf.jp/.
[15] B. Dolgoshein, Status report on silicon photomultiplier development and its applications, Nuclear Instrum. Methods Phys. Res. A 563 (2006) 368–376.
[16] A. Tsunesaburo, M. Masayoshi, O. Masayuki, Decay properties of ZnS(Ag) phosphors, J. Phys. Soc. Japan 14 (12) (1959) 1766–1770.
[17] S. Shiqekazu, S. Satoshi, Y. Kenichiro, Phoswich detectors for simultaneous counting of a, b, g-rays, and neutrons, Nuclear Instrum. Methods Phys. Res. A 388 (1997) 193–198.
[18] G.F. Knoll, Radiation Detection and Measurement, John Wiley and Sons, New York, 1999.
[19] K.M. Pritchard, A.N. Osovizky, J.B. Ziegler, E. Binkley, P. Tsai, N. Hadad, M. Jackson, C. Hurlbut, G.M. Baltic, C.F. Majkrzak, N.C. Maliszewskyj, Computational techniques for optimizing performance of a 6LiF:ZnS(Ag) neutron detector using recorded waveforms, in press.
[20] A.C. Stephan, S. Dai, S.A. Wallace, Neutronics aspects of position sensitive neutron scintillator detectors using wavelength shifting readout fibers, Appl. Radiat. Isot. 61 (2004) 1375–1382.
[21] H. Iwase, M. Katagiri, M. Shibayama, Optimization of the thickness of a ZnS/6LiF scintillator for a high resolution detector installed on a focusing small angle neutron scattering spectrometer, Appl. Crystallogr. 45 (2012) 507–512.
[22] J.-B. Mosset, A. Stoykov, U. Greuter, Evaluation of two thermal neutron detection units consisting of ZnS/6LiF Scintillating layers with embedded WLS fibers read out with a SiPM, Nuclear Instrum. Methods Phys. Res. A 764 (2014) 299–304.
[23] S. Agostinelli, J. Allison, K. Amako, Geant4 - a simulation toolkit, Nuclear Instrum. Methods Phys. Res. A 506 (2003) 250–303.
[24] Kuraray, Japan, 1–1. http://hallaweb.jlab.org/experiment/PVDIS/SoLID/EC/meetings/kuraray/Absorption&Emission%20of%20Y7811-1.pdf.[Online].
[25] http://multimedia.3m.com/mws/media/285747O/vikuiti-tm-ar-literature.pdf.
[26] http://alanod.com/sites/default/files/MIRO_SILVER_PD_8s_FINAL_D_E_11_14.pdf [Online].
[27] H. Iikura, N. Tsutsui, T. Nakamura, Evaluation of new lif-scintillator and optional brightness enhancement films for neutron imaging, Nuclear Instrum. Methods Phys. Res. A 651 (2011) 100–104.
[28] K.T. Rasoul, N.K. Abbas, Z.J. Sharan, Structural and optical characterization of Cu and Ni doped ZnS nanoparticles, Int. J. Electrochem. Sci. 8 (2013) 5594–5604.
[29] SensL, Ireland, J-Series Family, [Online].